Supporting Information

A Multi-Process Model for Photocatalytic Reduction of CO_2

Chen Sun, Yimin Xuan*, Kai Zhang

School of Energy and Power Engineering, Nanjing University of Aeronautics and Astronautics, Nanjing 210001, China.

E-mail: ymxuan@nuaa.edu.cn

1. Methods

1.1 DFT calculation

The generalized gradient approximation (GGA) of Perdew–Burke–Ernzerhof (PBE) is employed with the projected augmented-wave method for electronic exchange and correlation[1]. The kinetic cutoff energy for the plane-wave basis is set to 450 eV. During the model relaxing process, the threshold values of total electronic energies and the residual are set to 10^{-6}eV and 0.05 eV /Å respectively. The Gaussian smearing method was used with the width of smearing equal to 0.05eV. Transition-State (TS) searches are calculated using the climbing image nudged elastic band (CI-NEB)[2, 3]. The DFT-D3 method of Grimme was employed to describe the van der Waals (vdW) interaction[4]. The dielectric tensor is obtained using DFT calculations, the GW method[5], and the Bethe-Salpeter Equation (BSE)[6]. The band structure is calculated with the PBE0 and Heyd-Scuseria-Ernzerhof (HSE)[7].

To examine the stability of the catalysts structures, we also performed NVT Born–Oppenheimer AIMD (Ab-initio Molecular Dynamics) calculation with the temperature controlled using Langevin thermostat of friction coefficient of 10 ps^{-1}. All simulations run for 10000 steps (10 ps), with the data collection starting after 1000 steps of equilibration.

1.2 GW-Bethe Salpeter calculations

The widely used density functional theory (DFT) fails to predict the band gaps since there exists no formal justification to interpret the DFT eigenvalues as quasiparticle (QP) energies[8]. To solve this problem, the GW approximation is widely used, which generates better values for quasiparticle energies. GW quasiparticle calculations were carried out using the perturbative G_0W_0 approximation, starting from Hybrid wavefunctions and eigenvalues as

described above. The energy cutoff for the function was set to 150eV and increasing it up to 480eV without changing the results for a fixed number (174) of empty bands. Calculations of the macroscopic dielectric tensor within the BSE framework are performed starting from G_0W_0 eigenvalues. The k-point mesh is set as 16×16×1 Gamma-centered Monkhorst-packs in the calculation of the BSE spectra. The BSE Hamiltonian is formed using the 6 highest valence bands and the 8 lowest conduction bands using the Tamm-Dancoff approximation, and the dielectric tensor is output on the energy grid(3000 points) up to 6eV.

1.3 Carrier transport

The carrier recombination includes the radiative recombination and the non-radiative recombination. On the non-equilibrium condition, the radiative recombination rate can be expressed as[9]:

$$R_c = R_{c0}\frac{np}{n_0 p_0} \qquad (1)$$

where R_{c0} is the semiconductor recombination rate in thermal equilibrium, n_0 and p_0 are the quasi-equilibrium concentrations of electrons and holes.

Non-radiative recombination mainly consists of Auger recombination, Shockley-Read-Hall (SRH) recombination, and surface recombination[10]. For Auger recombination, the rate of it can be expressed as:

$$R_a = \left(C_n n + C_p p\right)\left(np - n_{i,eff}^{\ 2}\right) \qquad (2)$$

where C_n and C_p are the electron and hole Auger recombination coefficients, respectively. $n_{i,eff}$ is the effective intrinsic concentration of carrier, expressed as:

$$n_{i,eff} = \sqrt{N_{c0}N_{v0}}exp\left(-\frac{E_g}{2k_b T}\right) \qquad (3)$$

where N_{c0} and N_{v0} are effective state densities of conduction band and valence band, E_g is bandgap, k_b is boltzmann's constant, and T is temperature.

The rate of SRH recombination can be expressed as:

$$R_s = \frac{np - n_{i,eff}}{\tau_p n + \tau_n p} \qquad (4)$$

where τ_p and τ_n are lifetime of hole and electron, respectively.

The quantity of photogenerated charge carriers is conserved in the whole photocatalytic processes, the equation of carrier conservation can be obtained:

$$R_g = R_c + R_a + R_s + R_r + R_{suf} \qquad (5)$$

where R_r is the rate of surface reaction, R_{suf} is the rate of surface recombination.

For the sake of simplicity, $R_g - R_c - R_a - R_s$ is defined as R_1. In our model, the value of $R_r + R_{suf}$ is equal to R_1 according to Eqn.(5). If $R_r \leq R_1$, the R_{suf} will be set to $R_1 - R_r$ in the next step of iterative calculation. Oppositely, R_r is equal scale reduced to R_1 in the iterative calculation.

1.4 Mirco-kinetic Model

We employe a microkinetic model for the CO_2 and H_2 reduction reaction on the catalyst surface. In this model, the gaseous CO_2 molecules dissolved in the solution depends on the pressure and temperature, given by,

$$CO_{2(g)} \underset{k_{-1}}{\overset{k_{+1}}{\rightleftarrows}} CO_{2(aq)} \qquad (6)$$

where the equilibrium *K* is given as:

$$K_0 = \frac{c_{co_2}}{f_{co_2}} = exp\left\{93.4517\left(\frac{100}{T}\right) - 60.2409 + 23.3585ln\left(\frac{T}{100}\right)\right\} \qquad (7)$$

where c_{co_2} is the concentration of dissolved CO_2, and $f_{co_2}$is the fugacity of CO_2 in gas phase.

The dissolved CO_2 may then adsorb on the surface of the catalyst, given by

$$CO_{2(aq)} + * \underset{k_{-2}}{\overset{k_{+2}}{\rightleftarrows}} CO_2 * \qquad (8)$$

We performed ab initio DFT using the Vienna Ab Initio Simulation Package(VASP)[1, 11], and numerical simulation using COMSOL Multiphysics®, as detailed below.

After being adsorbed on the surface, CO_2 may be reduced to HCOOH by several proton-coupled electron transfer steps. The corresponding pair of reactions is given by

$$CO_2 * + H^+ + e^- \underset{k_{-3}}{\overset{k_{+3}}{\rightleftarrows}} OCHO * \qquad (9)$$

$$HCOO * + H^+ + e^- \underset{k_{-4}}{\overset{k_{+4}}{\rightleftarrows}} HCOOH * \qquad (10)$$

The CO_2 adsorbed on the surface also can be reduced to CO, given by

$$CO_2 * + H^+ + e^- \underset{k_{-5}}{\overset{k_{+5}}{\rightleftarrows}} COOH * \quad (11)$$

$$COOH * + H^+ + e^- \underset{k_{-6}}{\overset{k_{+6}}{\rightleftarrows}} CO * + H_2O \quad (12)$$

Alternatively, CO_2 can be reduced to CH_4, given by

$$CO * + H^+ + e^- \underset{k_{-7}}{\overset{k_{+7}}{\rightleftarrows}} CHO * \quad (13)$$

$$CHO * + H^+ + e^- \underset{k_{-8}}{\overset{k_{+8}}{\rightleftarrows}} CH_2O * \quad (14)$$

$$CH_2O * + H^+ + e^- \underset{k_{-9}}{\overset{k_{+9}}{\rightleftarrows}} CH_2OH * \quad (15)$$

$$CH_2OH * + H^+ + e^- \underset{k_{-10}}{\overset{k_{+10}}{\rightleftarrows}} CH_2 * + H_2O \quad (16)$$

$$CH_2 * + H^+ + e^- \underset{k_{-11}}{\overset{k_{+11}}{\rightleftarrows}} CH_3 * \quad (17)$$

$$CH_3 * + H^+ + e^- \underset{k_{-12}}{\overset{k_{+12}}{\rightleftarrows}} CH_4 * \quad (18)$$

Rather than by the reduction of CH_2O* as in Eq10, CH_2O can also be reduced to CH_3OH, given by

$$CH_2O * + H^+ + e^- \underset{k_{-13}}{\overset{k_{+13}}{\rightleftarrows}} OCH_3 * \quad (19)$$

$$OCH_3 * + H^+ + e^- \underset{k_{-14}}{\overset{k_{+14}}{\rightleftarrows}} CH_3OH * \quad (20)$$

We also consider the HER given by Volmer and Heyrovsky steps.

$$(Volmer) \qquad * + H^+ + e^- \underset{k_{-17}}{\overset{k_{+17}}{\rightleftarrows}} H * \quad (21)$$

$$(Heyrovsky) \qquad H * + H^+ + e^- \underset{k_{-18}}{\overset{k_{+18}}{\rightleftarrows}} H_2(g) \quad (22)$$

$$(Tafel) \qquad H * + H * \underset{k_{-19}}{\overset{k_{+19}}{\rightleftarrows}} H_2(g) \quad (23)$$

The dissociation of O_2 in one direct chemical step is also be included, given by

$$O_2 + * \underset{k_{-20}}{\overset{k_{+20}}{\rightleftarrows}} O* + O* \quad (24)$$

$$H^+ + e^- + * \underset{k_{-20}}{\overset{k_{+20}}{\rightleftarrows}} H* \quad (25)$$

$$OH^- + h^+ + * \underset{k_{-20}}{\overset{k_{+20}}{\rightleftarrows}} OH* \quad (26)$$

1.5 Continuum transport Model

The ionization equilibrium in solution are considered, as shown as:

$$CO_{2\,(aq)} + H_2O \underset{k_{-1}}{\overset{k_{+1}}{\rightleftarrows}} H^+ + HCO_3^-, pK_1 = 6.37 \quad (27)$$

$$HCO_3^- \underset{k_2}{\overset{k_{+2}}{\rightleftarrows}} H^+ + CO_3^{2-}, pK_2 = 10.25 \quad (28)$$

where *k* is the rate constant, and *K* is the reaction equilibrium constant.

1.6 Ratios of species in rGO−MoS_2/PPy

The molar ratio of MoS_2 and PPy is calculated by the data of synthesis. The synthesized rGO-MoS_2 (66 wt% of MoS_2 in 100mg) was added with 150 μL of pyrrole (98%)[12]. The mass fraction of MoS_2 and PPy(1 unit) are 160.07 and 65.09. In addition ,the density of liquid PPy is 0.9691g/ml. Herein, these are 0.412 mmol MoS_2 and 2.188 mmol PPy in one sample of rGO−MoS_2/PPy-150.

2. Supplementary Figures

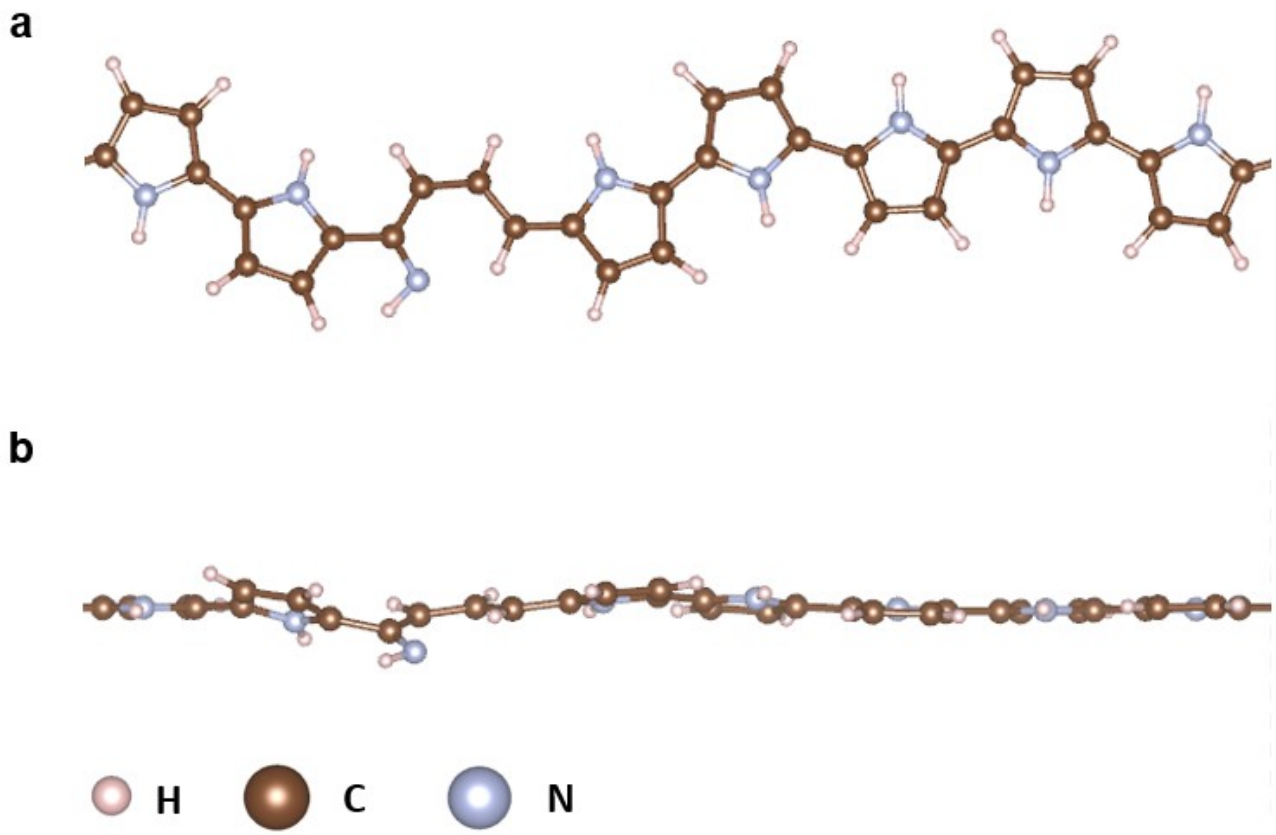

Figure S1. Structure of the PPy with C=N defect; (a)Top view;
(b)Front view

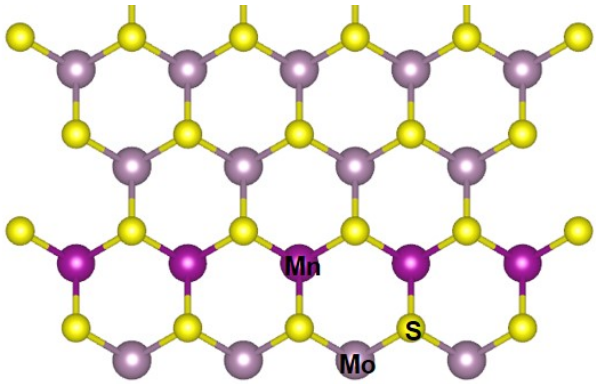

Figure S2. Structure of the m-MoS_2 with metal atom doped

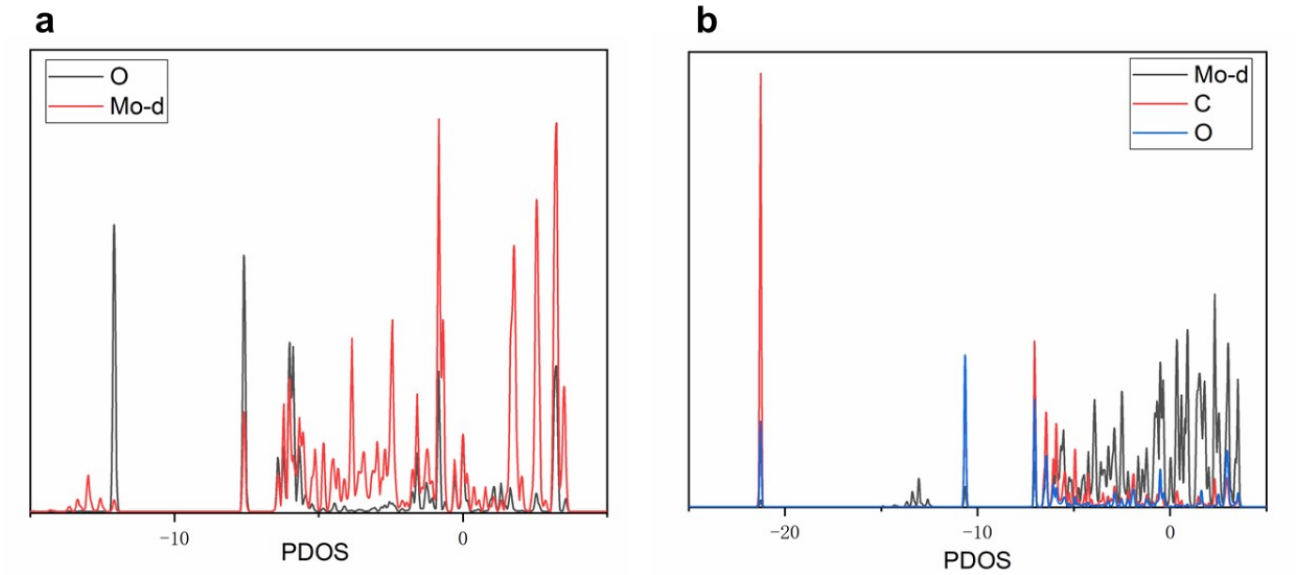

Figure S3. (a)PDOS of *COH absorbed on Mn doped MoS_2. (b) DOS of *CHO absorbed on Mn doped MoS_2

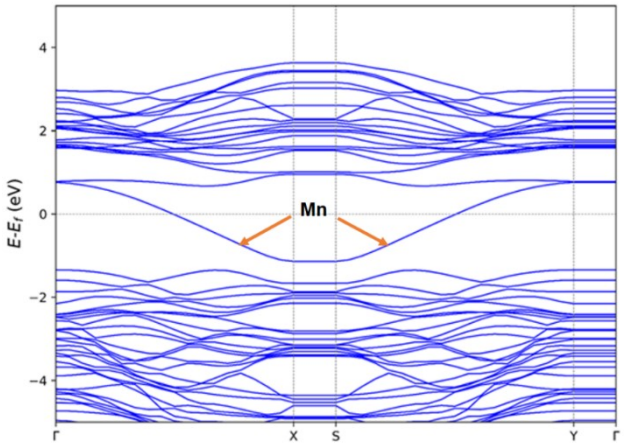

Figure S4. Band sturcture of Mn doped MoS_2

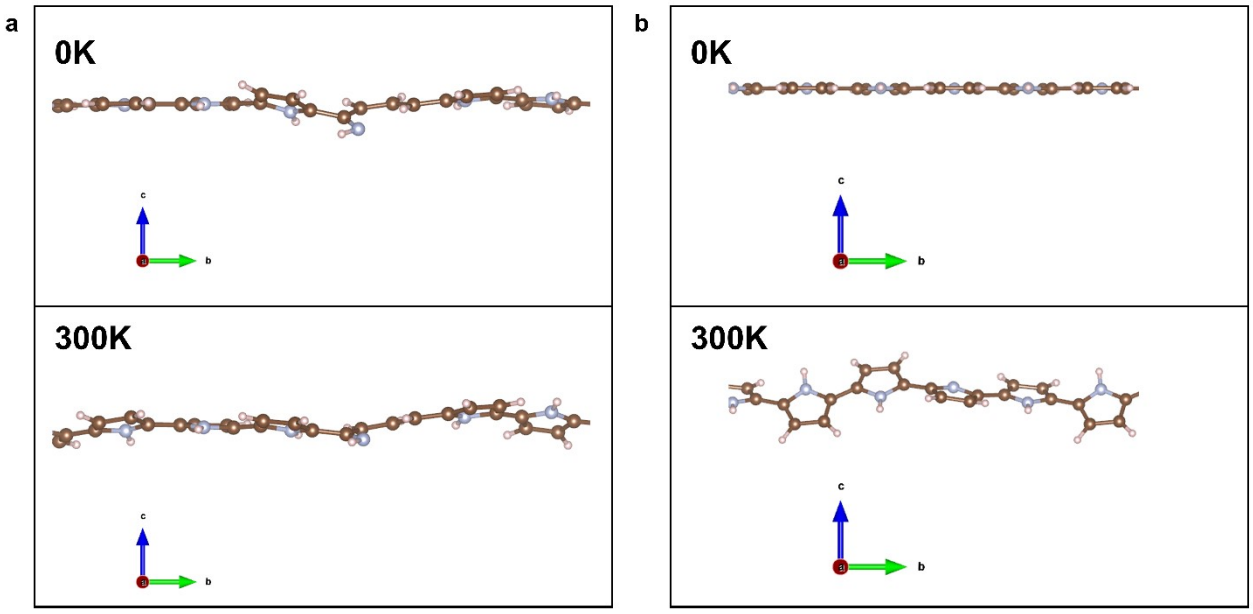

Figure S5. The results of AIMD simulations at 0K and 300K; (a) the AIMD simulation of Cd-PPy; (b) the AIMD simulation of PPy.

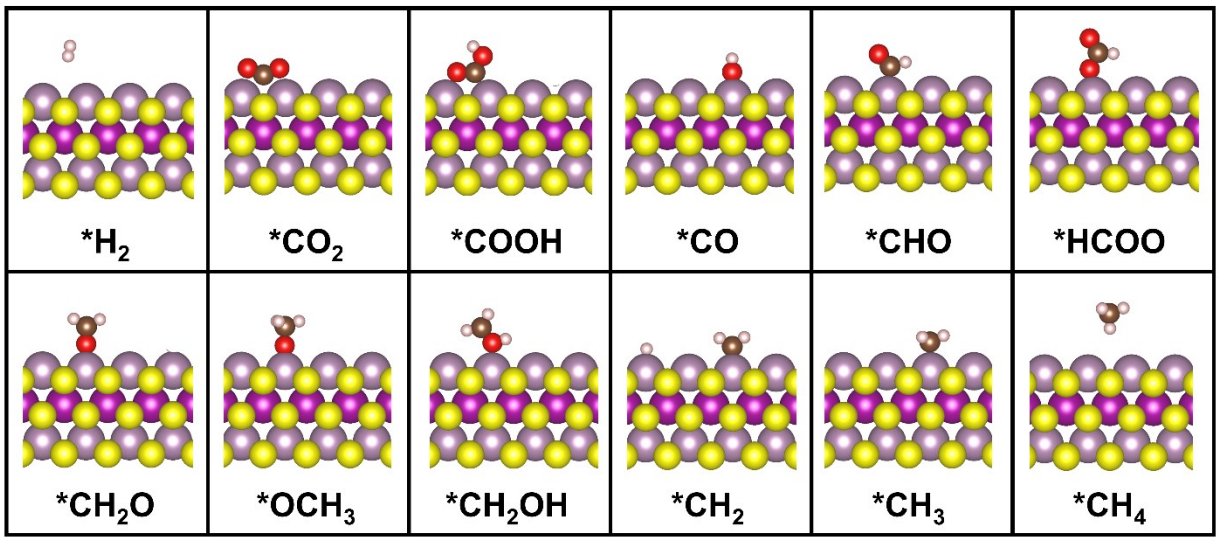

Figure S6. The structures of intermediates on $dMoS_2$.

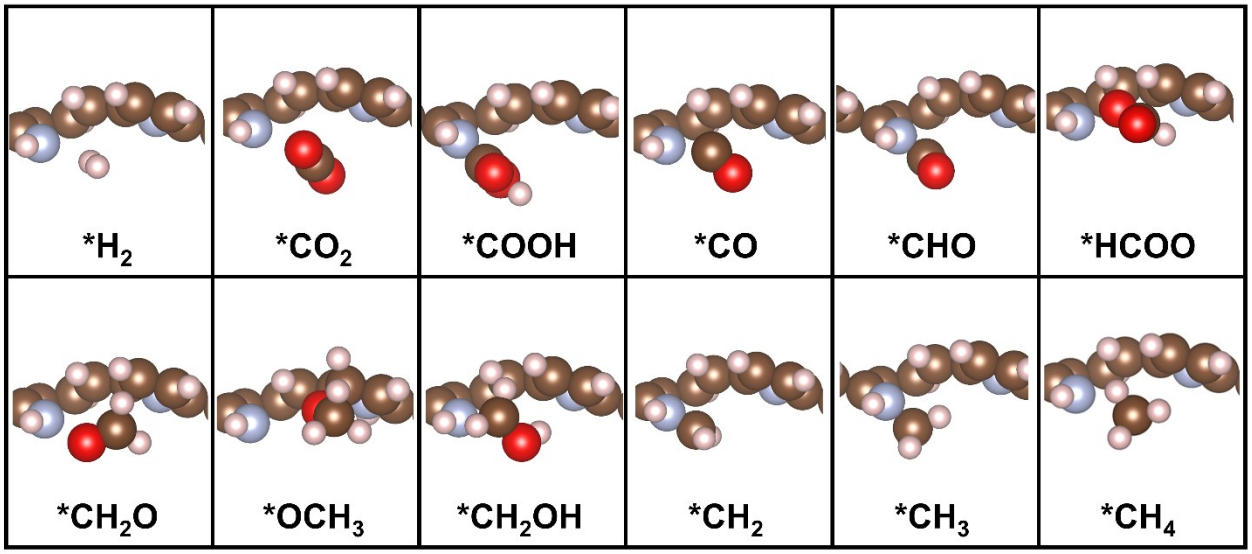

Figure S7. The structures of intermediates on Cd-PPy.

3. Supplementary Tables

Table S1. Adsorption of CO_2 on m-MoS_2, PPy and Cd-PPy

	$\Delta G_{ad}(eV)$
m-MoS_2	-1.68
PPy	-0.12
Cd-PPy	-0.77

Table S2. Diffusion coefficients of species in H_2O at 300K[13-15].

Species	Diffusion Coefficient ($10^{-9}m^2s^{-1}$)
CO_2	1.910
HCO_3^-	1.185
CO_3^{2-}	0.923
H^+	9.311
OH^-	5.273
H_2	5.11

CO	1.57
HCOOH	1.52
CH_3OH	1.28
CH_4	1.84
O_2	2.42

Reference

1. J. P. Perdew, K. Burke and M. Ernzerhof, *Physical Review Letters*, 1996, **77**, 3865-3868.
2. D. Sheppard, P. Xiao, W. Chemelewski, D. D. Johnson and G. Henkelman, *J Chem Phys*, 2012, **136**, 074103.
3. R. M. Henkelman, G. J. Stanisz and S. J. Graham, *J Magn Reson Imaging*, 2000, **11**, 568.
4. S. Grimme, J. Antony, S. Ehrlich and H. Krieg, *J Chem Phys*, 2010, **132**, 154104.
5. M. S. Hybertsen and S. G. Louie, *Phys Rev B Condens Matter*, 1986, **34**, 5390-5413.
6. G. Onida, L. Reining and A. Rubio, *Reviews of Modern Physics*, 2002, **74**, 601-659.
7. J. Heyd, G. E. Scuseria and M. Ernzerhof, *The Journal of Chemical Physics*, 2006, **124**.
8. M. Shishkin and G. Kresse, *Physical Review B*, 2006, **74**.
9. W. Van Roosbroeck and W. Shockley, *Physical Review*, 1954, **94**, 1558-1560.
10. P. T. Landsberg, *Nature*, 1978, **275**, 270-271.
11. P. E. Blochl, *Phys Rev B Condens Matter*, 1994, **50**, 17953-17979.
12. N. Kumar, S. Kumar, R. Gusain, N. Manyala, S. Eslava and S. S. Ray, *ACS Applied Energy Materials*, 2020, **3**, 9897-9909.
13. M. Flury and T. F. Gimmi, *6.2 Solute Diffusion*, Methods of Soil Analysis, Part 4, Physical Methods, 2002.
14. D. W. H. Rankin, *CRC handbook of chemistry and physics, 89th edition, edited by David R. Lide*, 2009.
15. B. Jähne, G. Heinz and W. Dietrich, *Journal of Geophysical Research*, 1987, **92**.